

Abstract

Acoustic-gravity waves (AGWs) produced by earth-based natural hazards, anthropogenic events, or space-based events propagate into the ionosphere and cause anomalous waveforms, or traveling ionospheric disturbances (TIDs). These can be measured with Global Navigation Satellite System (GNSS) total electron content (TEC) measurements (Mannucci et al., 1998)(Kaladze et al., 2008). With the launch of the Jet Propulsion Laboratory's GUARDIAN system (<https://guardian.jpl.nasa.gov>) (Martire et al., 2022) on 2022-09-15, we now have access to filtered slant TEC observations. Currently, TEC measurements are computed for more than 90 GNSS ground stations that monitor the four main GNSS constellations (GPS, Galileo, BeiDou, and GLONASS). This system supports the development of near-real-time (NRT) ionospheric monitoring of potential disturbances due to natural or anthropogenic events on Earth. Our previous research has shown the success of implementing an LSTM-based algorithm to detect a local AGW disturbances in the ionosphere ten minutes after an earthquake event. This research expands the previous case study to GNSS stations distributed across the South Pacific, searching across a two-month time period 2023-05-01 to 2023-07-01. The results hope to show detection of open ocean earthquake events and the feasibility of NRT ionospheric monitoring over large regions with minimal stations.

Observation of seismic AGWs disturbing the ionosphere with GNSS has been proven by extensive studies using TEC measurements from GNSS observation data to detect AGW disturbance within the ionosphere after earthquake events such as the March 11, 2011 (UTC) Tohoku earthquake (Occhipinti et al., 2013) (Rolland et al., 2011), and the July 4, 2019 (UTC) Ridgecrest earthquake (Sanchez et al., 2022). GNSS signal differential delay measures Slant TEC in units $10^{16} \text{el}/\text{m}^2$. Slant TEC data is filtered with the fourth-order Butterworth high pass filter, removing frequencies below 1.1 mHz (Martire et al., 2022).

$$\text{Slant TEC} \approx \frac{f_1^2 f_2^2}{K(f_1^2 - f_2^2)} (\phi_{f_1} - \phi_{f_2})$$

K is a constant, approximating the plasma frequency ($\approx 40.308193 \text{m}^3 \text{s}^{-2}$), $f_{1,2}$ are the carrier frequencies, and $\phi_{1,2}$ are the measured phases along the respective frequencies (Teunissen and Montenbruck, 2017)

References

Kaladze, T., Pokhotelov, O., Shah, H., Khan, M., and Stenflo, L. (2008). Acoustic-gravity waves in the earth's ionosphere. *Journal of atmospheric and solar-terrestrial physics*, 70(13):1607-1616.

Mannucci, A. J., Wilson, B. D., Yuan, D. N., Ho, C. H., Lindqvist, U. J., and Runge, T. F. (1998). A global mapping technique for gps-derived ionospheric total electron content measurements. *Radio science*, 33(3):565-582.

Martire, L., Krishnamoorthy, S., Vergados, P., Romans, L. J., Szilagyi, B., Meng, X., Anderson, J. L., Komjáthy, A., and Bar-Sever, Y. E. (2022). The guardian system—a gnss upper atmospheric real-time disaster information and alert network. *GPS Solutions*, 27(1):1521-1886.

Occhipinti, G., Rolland, L., Lognonné, P., and Watada, S. (2013). From Sumatra 2004 to tohoku-oki 2011: The systematic gps detection of the ionospheric signature induced by tsunamigenic earthquakes. *Space Physics*, 118(6):3626-3636.

Rolland, L. M., Lognonné, P., Astafeyeva, E., Kherani, E. A., Kobayashi, N., Mann, M., and Muneke, H. (2011). The resonant response of the ionosphere imaged after the 2011 off the pacific coast of tohoku earthquake. *Earth, planets, and space*, 63(7):853-857.

Sanchez, S. A., Kherani, E. A., Astafeyeva, E., and de Paula, E. R. (2022). Ionospheric disturbances observed following the ridgecrest earthquake of 4 July 2019 in California, USA. *Remote sensing (Basel, Switzerland)*, 14(1):188-.

Teunissen, P. and Montenbruck, O. (2017). *Springer Handbook of Global Navigation Satellite Systems*. Springer Handbooks. Springer International Publishing, Cham, 1st ed. 2017. edition.

Set up

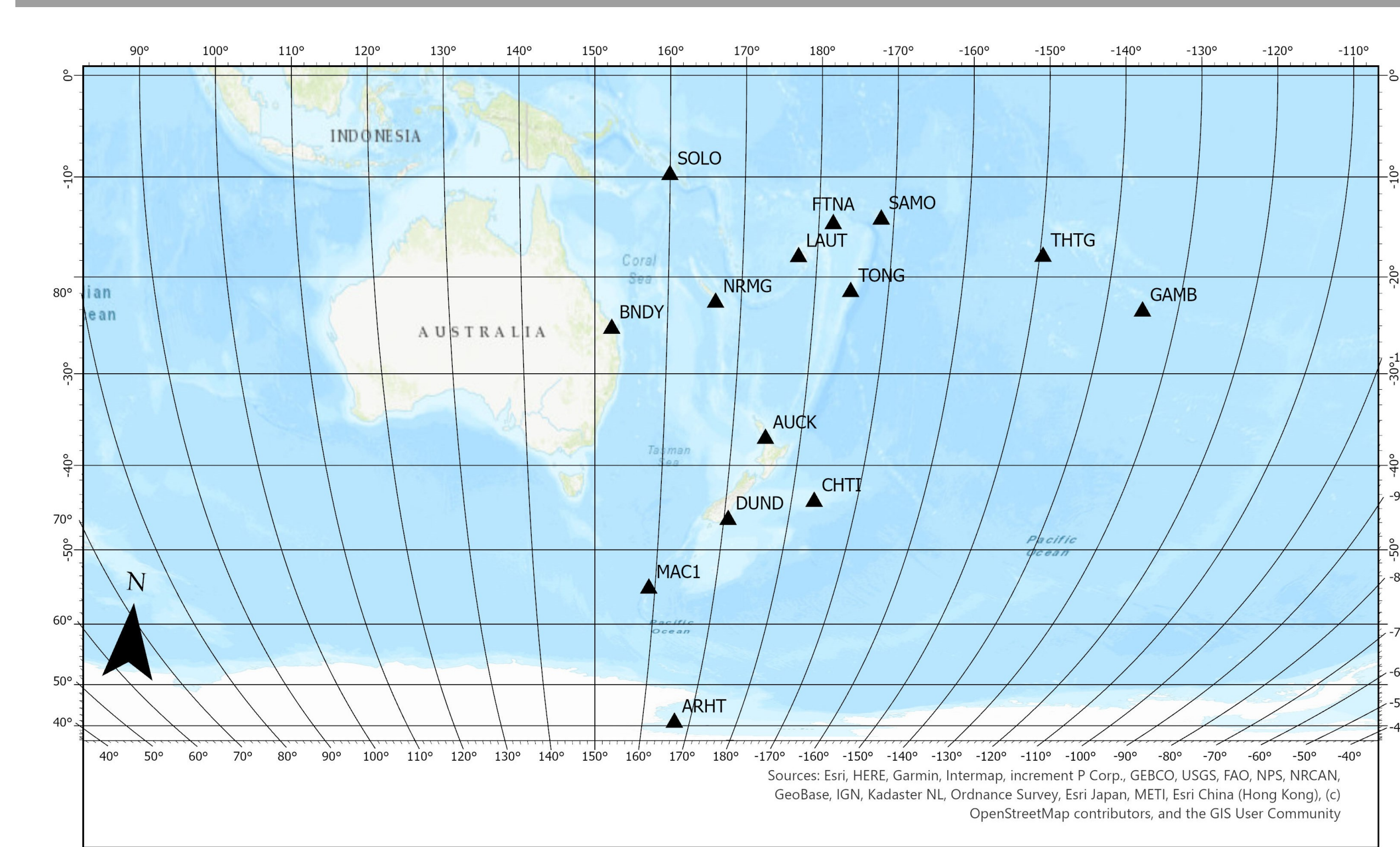


Figure 1: Fourteen station locations across the South Pacific were used for testing the ionospheric anomaly detection method. Three stations, LAUT, AUCK, ARHT are used as training for the LSTM prediction model.

Filtered TEC time series data is available from fourteen stations in the GUARDIAN network between 2023-01-01 to 2023-07-01. Filtered TEC time series data from three stations, LAUT, AUCK, and ARHT, between 2023-01-01 to 2023-05-01 is used to train three Long Short-Term Memory (LSTM) TEC prediction models. These three models are used to generate TEC predictions for the network of fourteen stations between 2023-05-01 to 2023-07-01. These two months are considered the test data set.

Process flow diagram:

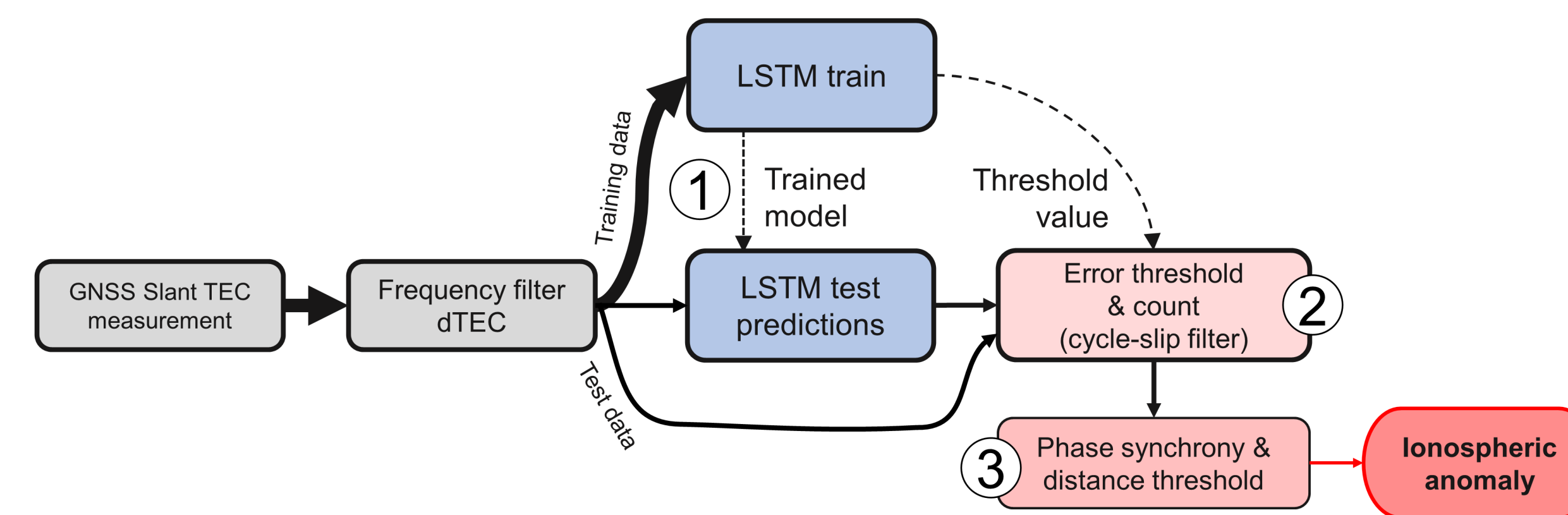


Figure 2: Process flow diagram for ionospheric anomaly detection method

Test data is streamed in 10-minute intervals with 5-minute overlaps, simulating a real-time data stream scenario.

Events of interest

Earthquake events of interest during test period May and June for this research

- May 10 2023, M 7.6, Tonga, Niutoputapu offshore
- May 19 2023, M 7.7 New Caledonia, Loyalty Islands offshore
- May 20 2023, M 7.1 New Caledonia, Loyalty Islands offshore
- June 15 2023, M 7.2 Tonga, Tongatapu offshore

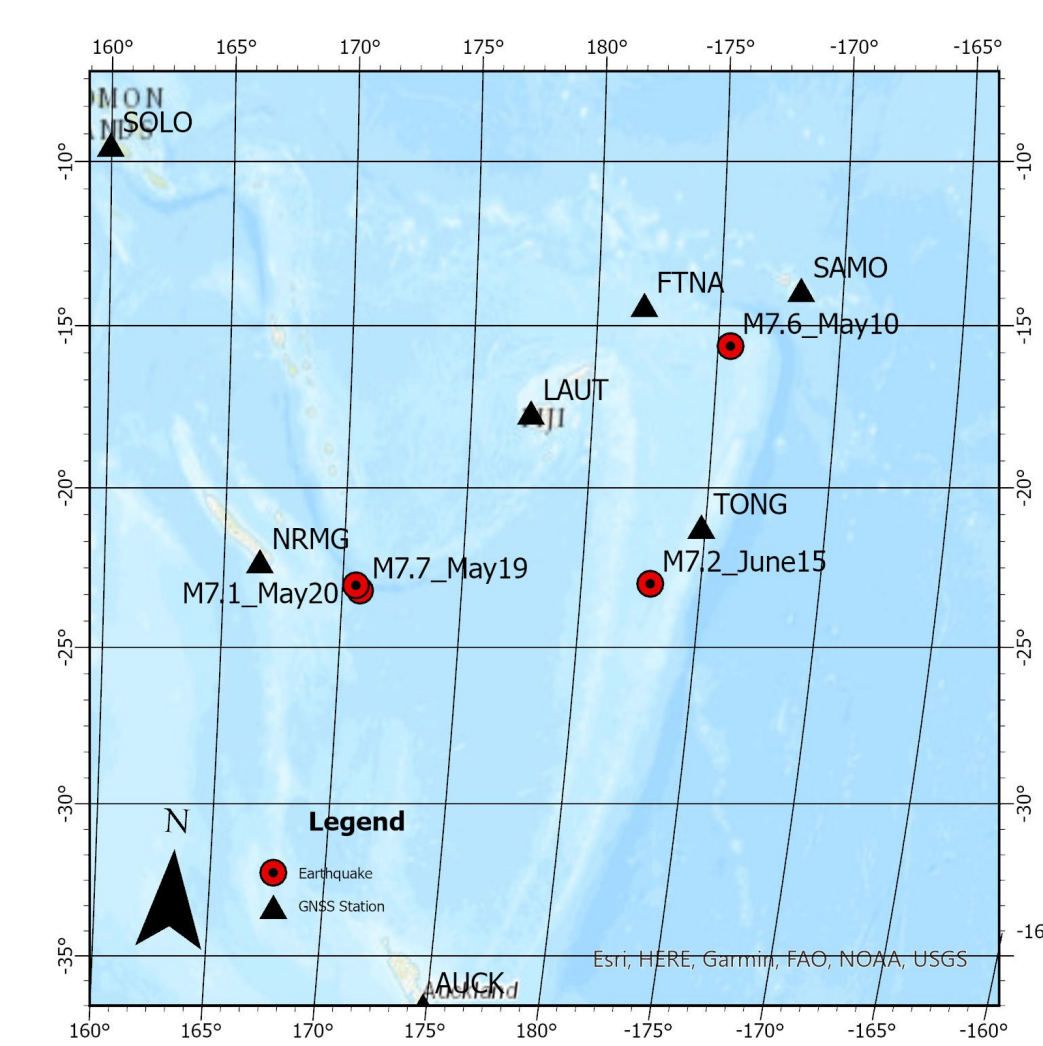


Figure 3

IN PROGRESS Preliminary Results

The following results are still IN PROGRESS. Not all stations have been run through testing. The detection methodology is still in progress and results may change in future publications.

Preliminary Results for Events of Interest

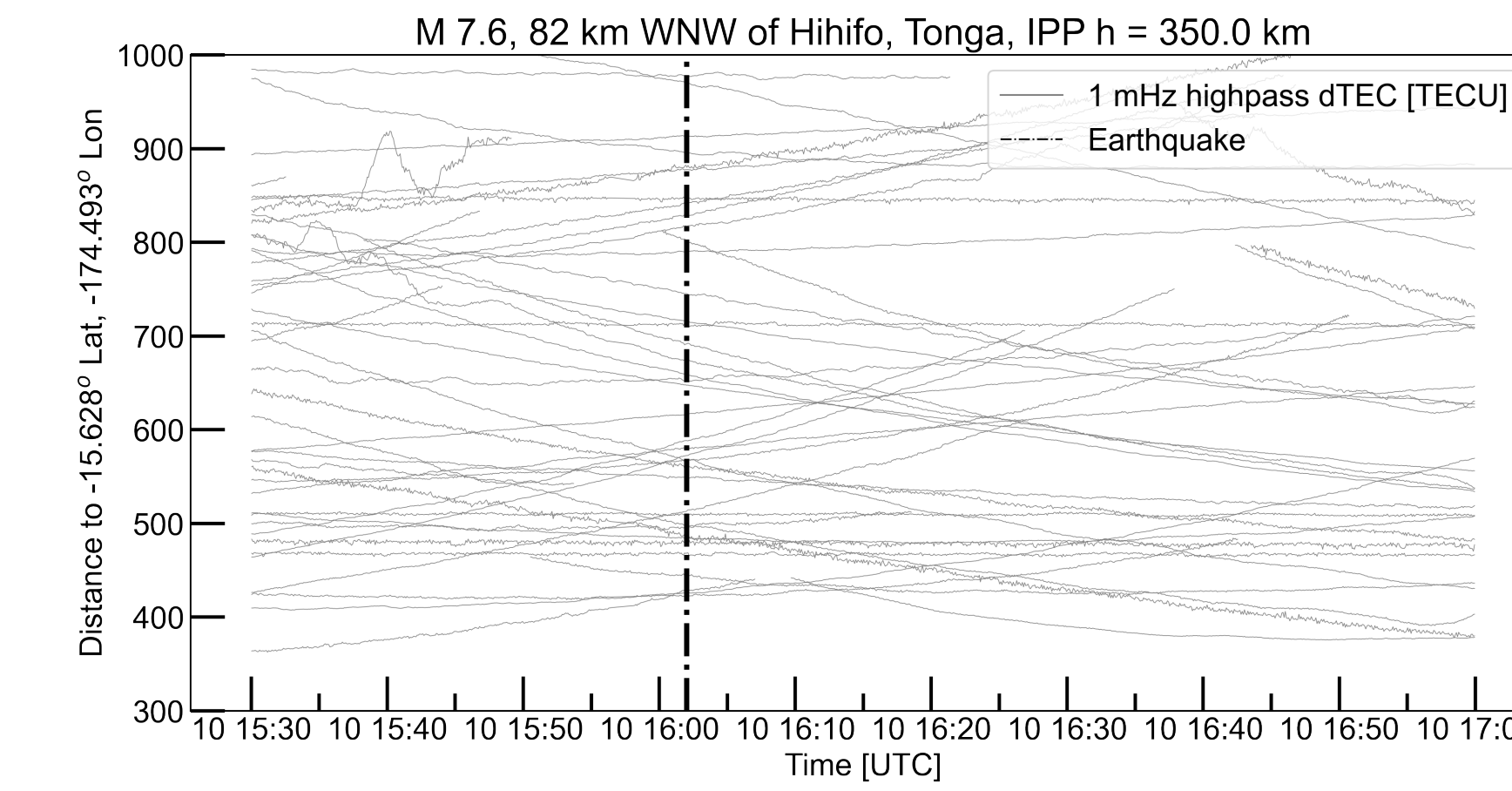


Figure 4: There was no GNSS recorded disturbance in ionosphere after the 2023 05 01 Earthquake with the select stations, therefore there were no anomalous behavior detections.

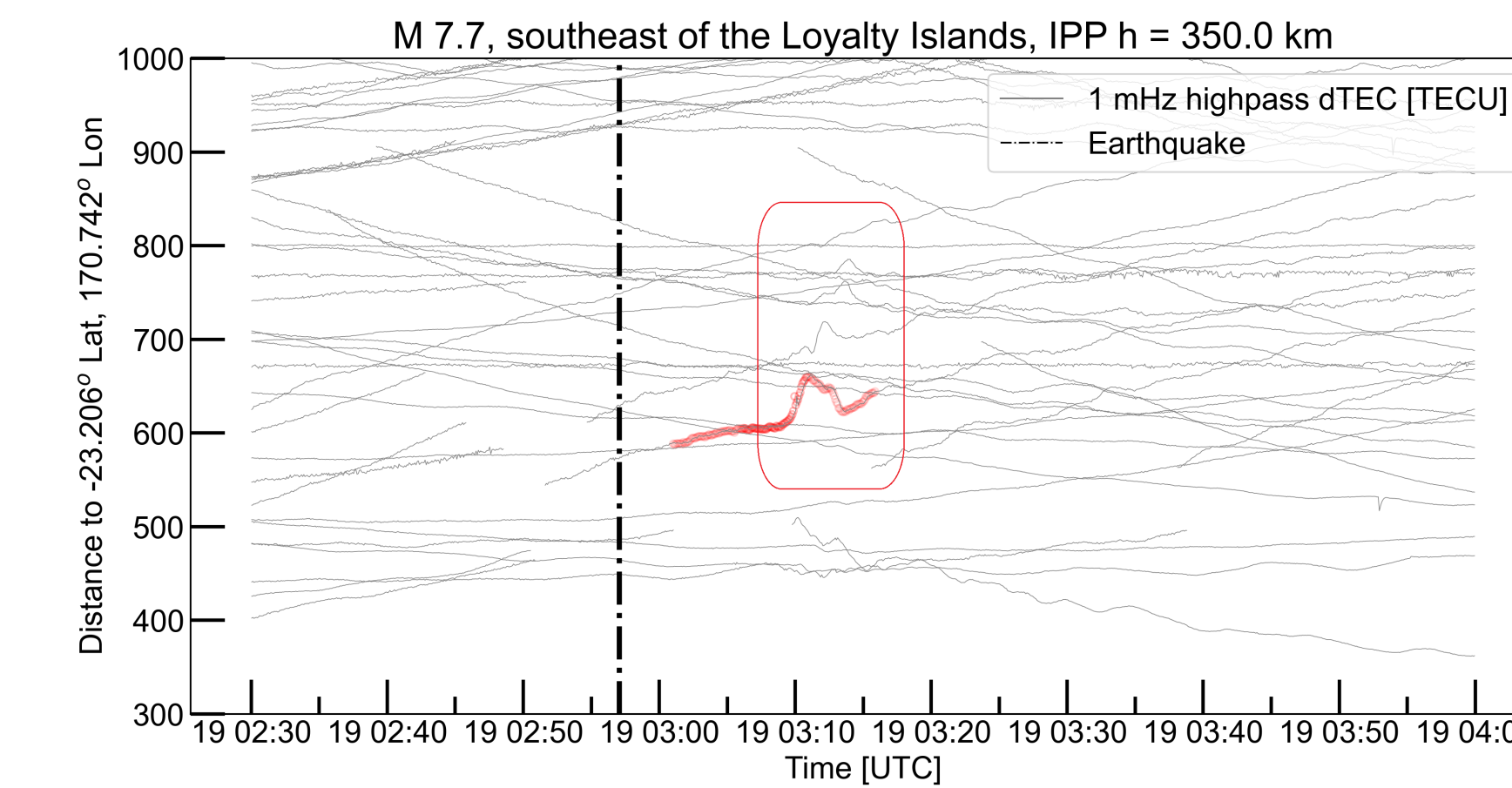


Figure 5: There is a visible disturbance in the data set, outlined with the red box, at the LAUT station across four satellites: C201M, C222M, R852, R859. Unfortunately only the LAUT-C201M TEC measurements exceeded the error threshold of 3σ and alerted to an anomaly. After the phase synchrony filter ran, this detection was removed from the final results due to it being the only error raised from this event.

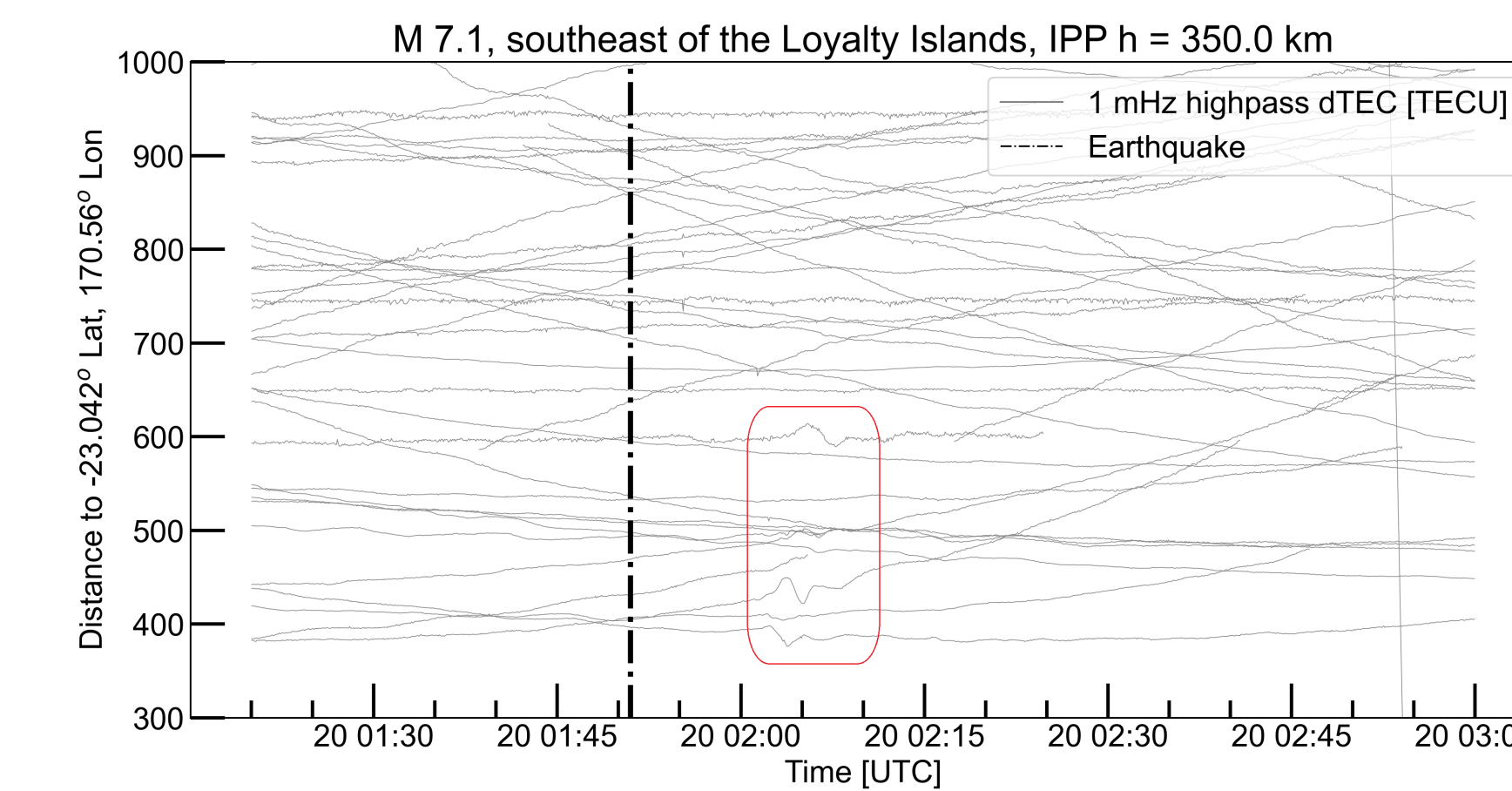


Figure 6: There is a visible disturbance, outlined with the red box, at three of the station-satellite TEC measurements. Each of these disturbances alerted to an anomalous behavior.

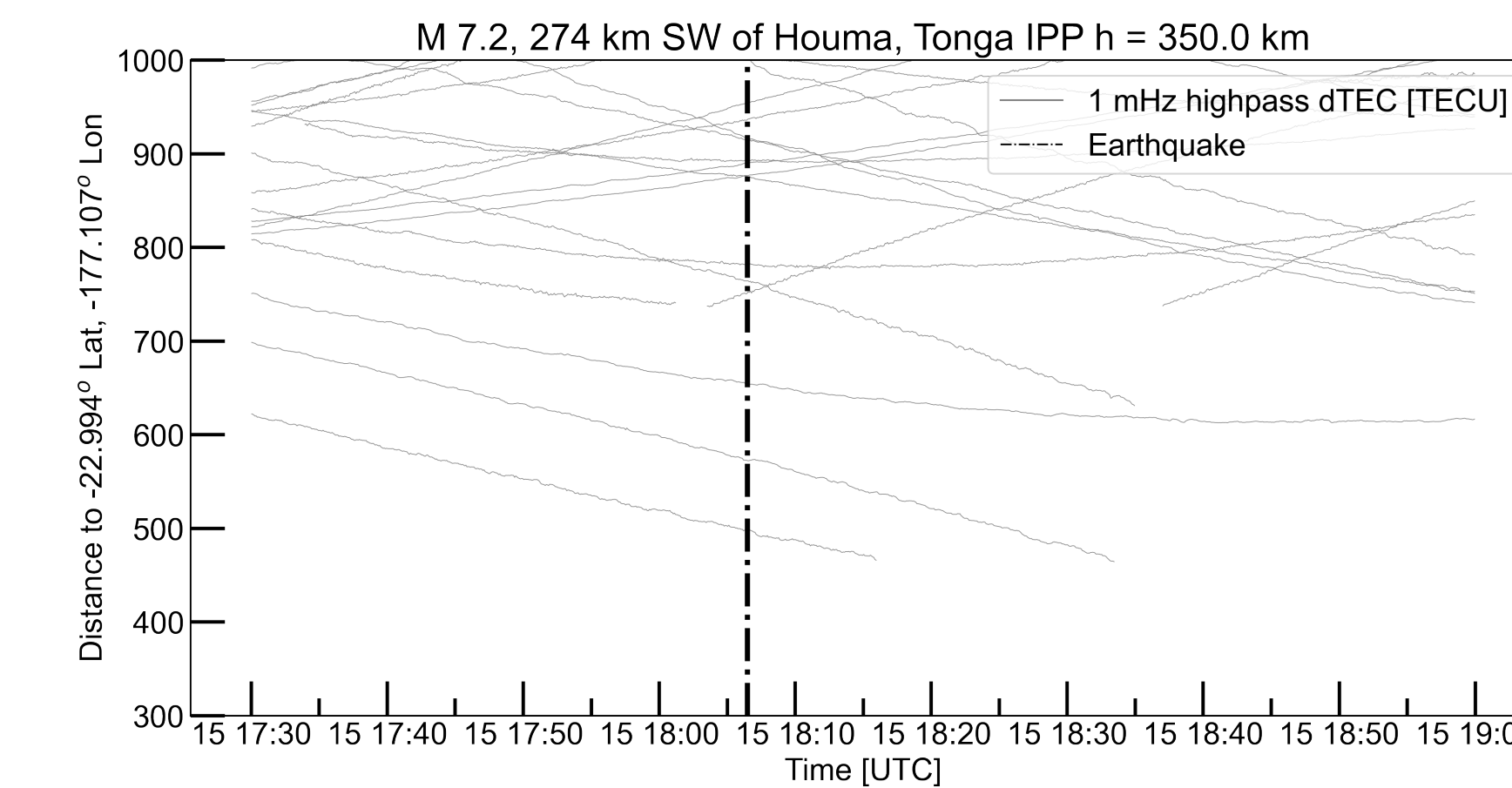


Figure 7: There is no visible ionospheric disturbance after this earthquake event likely due to the geometry of the available station-satellite pairs and lack of coverage.

Preliminary Results Overview

Although the error threshold filter did classify the disturbance after the M_w 7.7 earthquake on 2023 May 19 as anomalous, only one of the four disturbances triggered this alert. Therefore, when passed through the phase synchrony filter, this anomaly was dropped from the final results. Based on the final results, it is not surprising that detection of anomalous events due to open ocean earthquakes will prove difficult. There are many anomalous detections with much larger amplitude and duration than the co-seismic events.

Of note is the re-occurring anomaly detection between the UTC hours of 8:00 to 13:00 at stations FTNA, LAUT, and SAMO. The three examples shown in Figures 8, 11, and 14 reflect examples of this disturbance. This disturbance location is consistently over and to the north of Samoa and Fiji.

Preliminary Results Anomaly Detection Examples

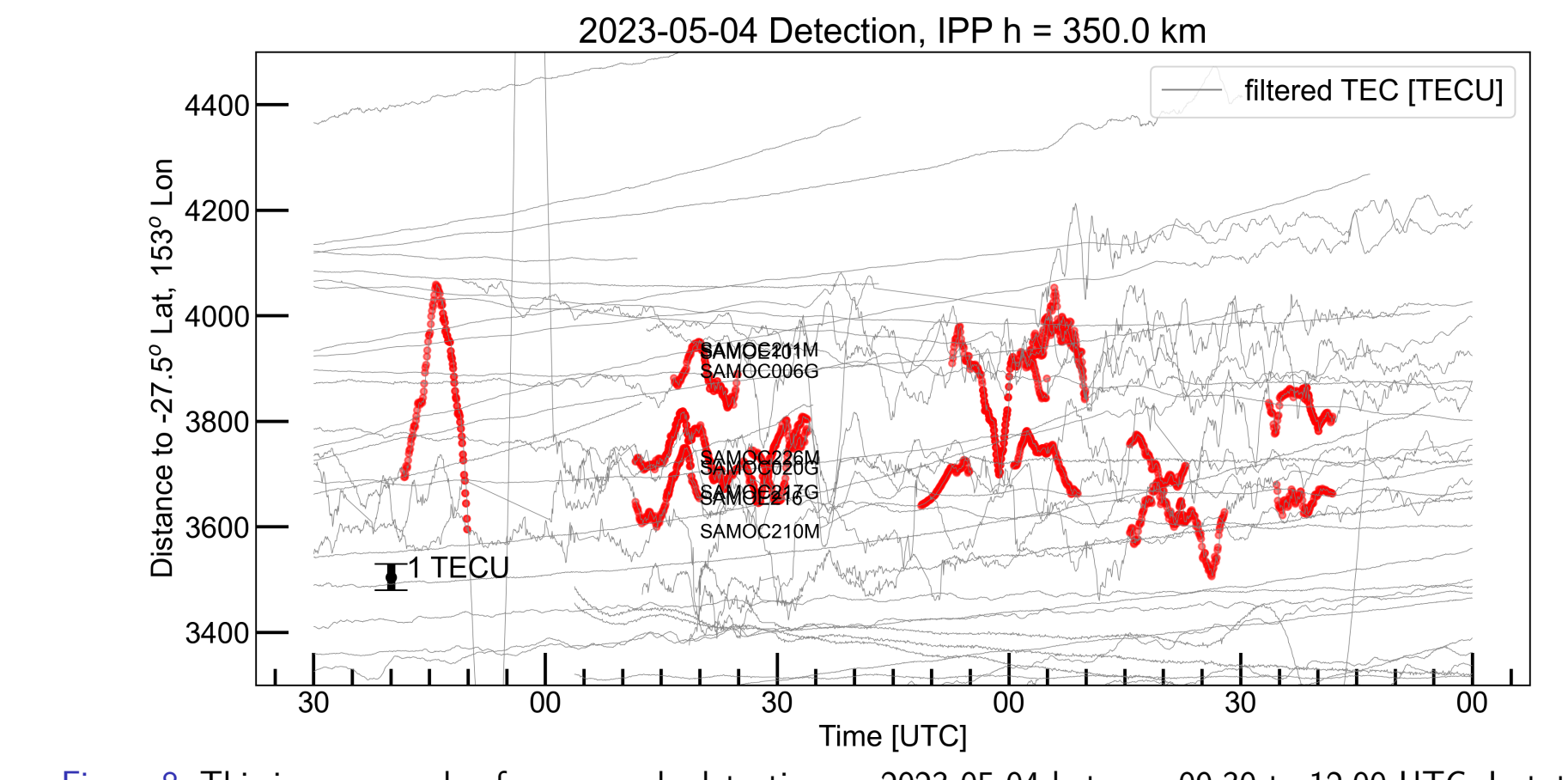


Figure 8: This is an example of an anomaly detection on 2023-05-04 between 09:30 to 12:00 UTC. In total, 8 signals were flagged as anomalous all from the station SAMO across constellations BeiDou and Galileo.

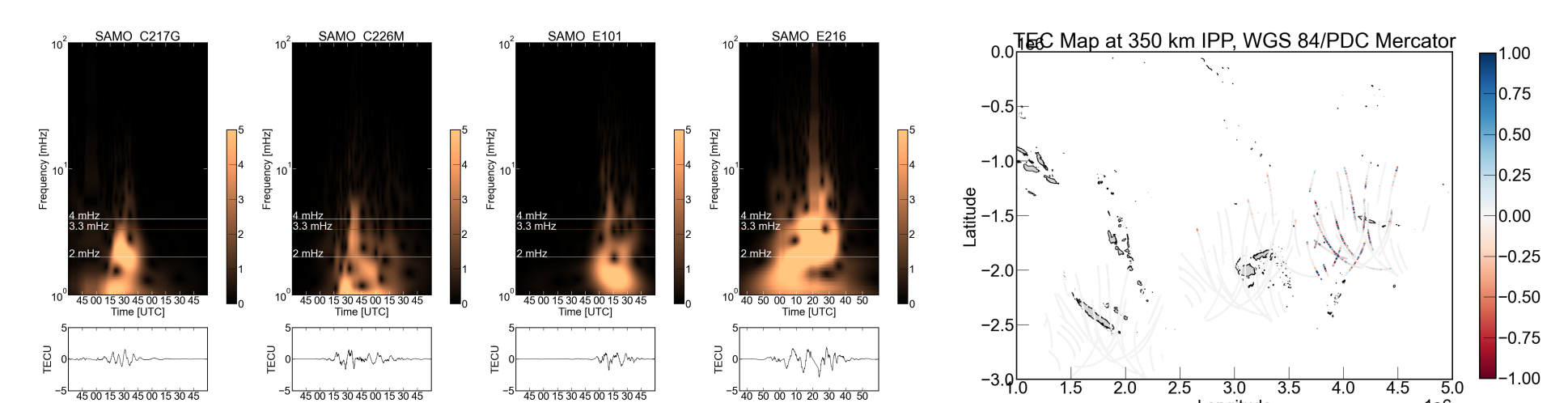


Figure 9: This shows the CWT analysis for the anomalous detection above. Frequencies are primarily in the gravity wave range with TECU amplitudes in the $\pm 1-2$ range.

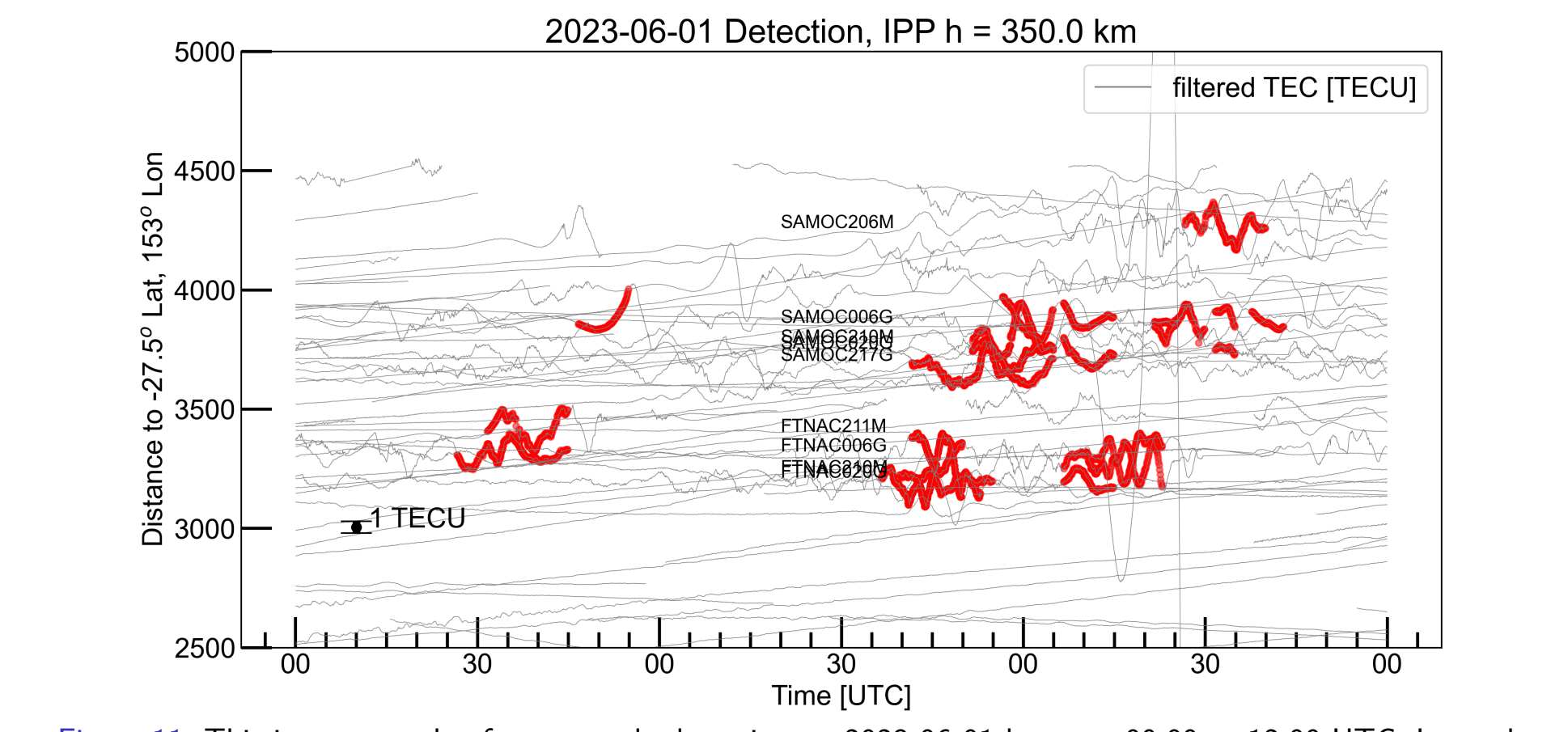


Figure 10: This shows the slant TEC IPP location of the anomalous detection.

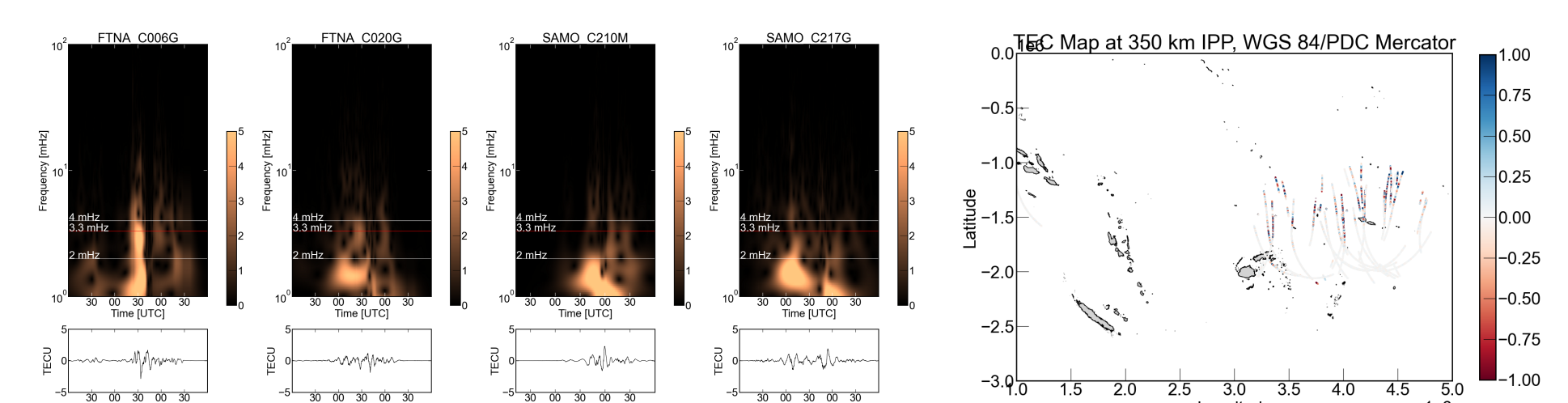


Figure 11: This is an example of an anomaly detection on 2023-06-01 between 09:00 to 12:00 UTC. In total, 9 signals were flagged as anomalous, 5 from the station SAMO and 4 from station FTNA. All signals were from BeiDou constellation.

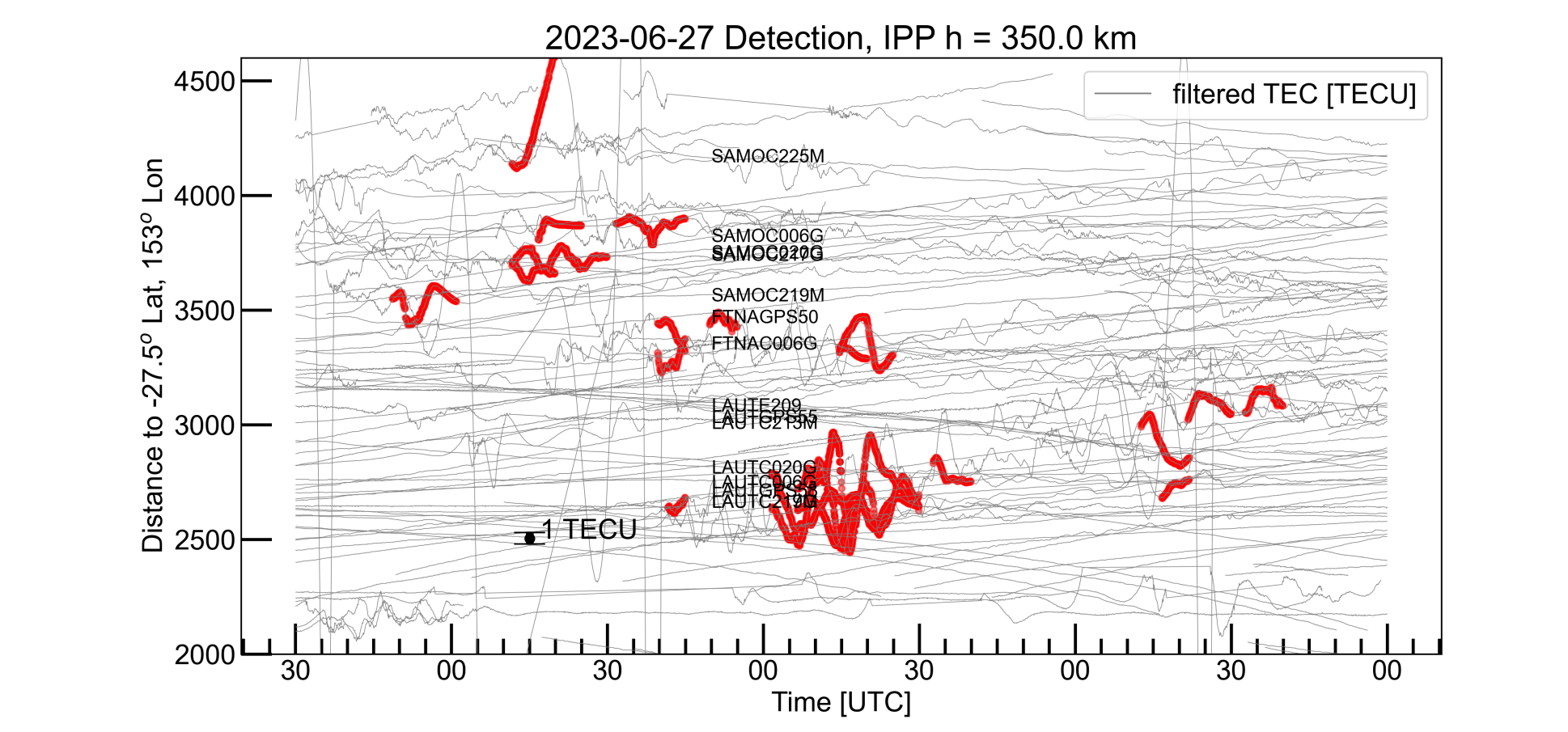


Figure 12: This shows the CWT analysis for the anomalous detection above. Frequencies are primarily between 1-2 mHz with TECU amplitudes in the $\pm 1-3$ range.

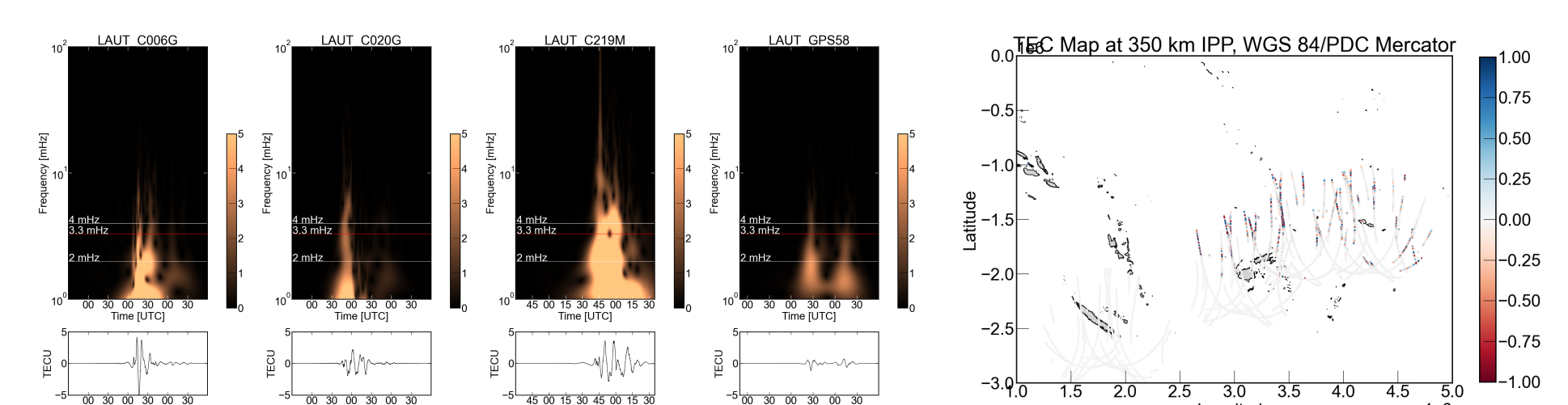


Figure 13: This shows the slant TEC IPP location of the anomalous detection.

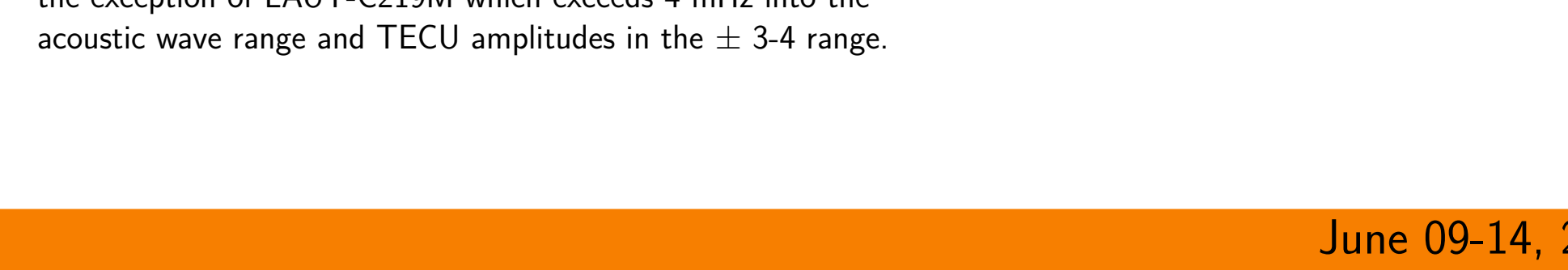


Figure 14: This is an example of an anomaly detection on 2023-06-27 between 09:30 to 13:00 UTC. In total, 9 signals were flagged as anomalous, 2 from the station FTNA, and 8 from station LAUT, and 5 from station SAMO. Signals were across BeiDou, GPS, and Galileo constellations.

Figure 15: This shows the CWT analysis for the anomalous detection above. Frequencies are primarily between 1-2 mHz with the exception of LAUT-C219M which exceeds 4 mHz into the acoustic wave range and TECU amplitudes in the $\pm 3-4$ range.

Figure 16: This shows the slant TEC IPP location of the anomalous detection.